Chinese Journal of Mechanical Engineering

ORIGINAL ARTICLE

Open Access

Local Stress Measurement in Thin Aluminum Plates based on Zero-Group-Velocity Lamb mode

Weiming Xuan, Maodan Yuan*, Xuanrong Ji*, Wenjin Xu, Yan Chen and Lvming Zeng

Abstract

The stress state is critical to the reliability of structures, but existing ultrasonic methods are challenging to measure local stress. In this paper, zero-group-velocity (ZGV) Lamb mode was proposed to measure the local stress field in thin aluminum plates. The Lamb wave's dispersive characteristics under initial stress were analyzed based on the Floquet-Bloch theory with Murnaghan hyperelastic material model. The obtained dispersion curves show that higher-order Lamb wave modes near the cut-off frequencies are sensitive to applied stress across the plate, indicating that the S1-ZGV mode has a rather high sensitivity to stress. Similar to conventional ultrasonic stress measurement, it is found that the frequency of the S1-ZGV mode changes near-linearly with the amplitude of applied stress. Numerical experiments were conducted to illustrate the feasibility of local stress measurement in a thin aluminum plate based on the S1-ZGV mode. Single and multiple localized stress fields were evaluated with the S1-ZGV method, and reconstructed results matched well with actual stress fields, proving that the ZGV Lamb wave method is a sensitive stress measurement technique in thin plates.

Keywords Stress field, Zero-group-velocity mode, Dispersion curves, Acoustoelastic effect, Lamb wave

1 Introduction

The stress state is an important indicator of the safety and reliability of engineering structures. It is more common for a structure to endure a certain degree of stress during mechanical processing and in practical service rather than staying in a stress-free state. Excessive stress, especially tensile stress on the surface layer, makes structures tend to increase crack initiation and propagation. Therefore, timely and accurate stress measurement is of great importance for the safety insurance of in-service structures [1].

*Correspondence:
Maodan Yuan
mdyuan@gdut.edu.cn
Xuanrong Ji
xr.ji@gdut.edu.cn
State Key Laboratory of Precision Electronic Manufacturing Technology and Equipment, Guangdong University of Technology, Guangzhou 510006, China

Among various nondestructive testing (NDT) techniques, ultrasonic testing has been proven effective for stress measurement based on the well-known acoustoelastic effects. The presence of initial stresses can bring in a small but non-negligible influence on the elastic wave propagation in solid media, including a variation of wave velocity, attenuation, and nonlinear phenomenon [2]. The ultrasonic method of measuring stress has been rapidly developed since Hughes and Kelly first put forward and experimentally verified the acoustoelastic effect of bulk waves [3]. According to different wave patterns, ultrasonic stress measurement can be further divided into the Rayleigh surface wave method [4, 5], the shear wave method [6], and the critically refracted longitudinal (Lcr) wave method [7]. Among these methods, Lcr wave is the most widely applied due to its high sensitivity to stress. Mohammadi et al. evaluated the stress level within elastic and plastic limits via the Lcr wave method and discussed

the influence of sensor distance on measurement accuracy [8].

Moreover, based on the fact that the penetration depth of the Lcr wave is related to its frequency, Javadi et al. used a series of transducers with different frequencies to evaluate the residual stress through the thickness in steel plates and welded stainless pipes [9, 10]. Sadeghi et al. measured residual stress in aluminum plates after friction stir welding using the Lcr waves method and validated numerical results from the finite element method [11]. However, due to the penetration depth, Lcr is only limited to evaluating the surface and the near surface of the tested specimen within one wavelength. Furthermore, it is not easy to accurately measure the local stress field because enough propagation distance is needed to extract the time shift of Lcr wave propagation under stress.

To pursue full coverage and improve the sensitivity of ultrasonic stress measurement, researchers expand the studies to the prestressed waveguide to investigate the effects of initial stress on various guided wave modes. Mohabuth et al. conducted theoretical research on the effects of uniform stress on the propagation of Lamb waves and reported a high sensitivity of phase velocity to the applied stress near the cut-off frequencies of higher-order Lamb wave modes [12]. Gandhi et al. provided a fairly comprehensive formulation of the acoustoelastic Lamb wave to analyze the effect of biaxial loading in initially isotropic plates [13]. Shi et al. measured phase velocity change depending on the propagation direction under applied biaxial loads using spatially distributed piezoelectric disks [14]. Pei and Bond numerically and experimentally demonstrated significantly higher sensitivity of higher-order Lamb modes to stress than the fundamental Lamb wave modes [15, 16]. Although higher-order Lamb modes show high sensitivity, it still needs a long inspection length to ensure accurate time-of-flight (ToF) to calculate the stress in plates. The long inspection length makes such measurement an averaging method of the stress field. It makes Lamb wave stress measurement based on ToF unable to evaluate nonuniform stress fields, which is much more common in a practical situation.

On the other hand, researchers found that there are special modes called zero group velocity (ZGV) modes that are most sensitive to the local properties of the inspected structures. ZGV Lamb mode has finite phase velocity while its group velocity becomes zero [17]. The vanish of group velocity is due to the interference of two modes with the same mode shape propagating with equal absolute phase velocities but with opposite directions. It means that the ZGV mode will not propagate far from the excitation position and only produce a local resonance. This stationary mode shows a local ringing resonance with a sharp and distinct frequency peak in the response spectrum. The elastic properties and thickness of the plate define the characteristics of ZGV modes. Up to now, ZGV modes have been widely used to quantitatively evaluate local material characteristics, including the thickness of concrete [18], bulk wave velocity and thickness of thin plates [19, 20], elastic constants of hollow cylinders [21], as well as the bond quality of layered structures [22, 23]. The literature mentioned above demonstrates that ZGV modes have high sensitivity to a local change in material properties, which shows us that ZGV Lamb modes have great potential for local stress measurement in thin plates. Although the application of ZGV modes is rather extensive, to the authors' best knowledge, stress measurement based on ZGV Lamb mode has not yet been conducted and reported.

This paper investigates the feasibility of measuring local stress with high sensitivity based on ZGV mode. The paper is organized as follows. Section 2 briefly introduces the theory of the Lamb wave acoustoelastic effect. Based on Floquet-Bloch (F-B) theory, Section 3 calculates and shows the dispersion curves of various Lamb wave modes with uniform initial stress, especially the effect on S1-ZGV mode. Section 4 illustrates local stress measurement for different stress fields using S1-ZGV modes in numerical experiments. Finally, concluding remarks are drawn in Section 5.

2 Theory of Lamb Wave Under Initial Stress

This section briefly introduces the general theory for Lamb wave acoustoelastic effect in stressed plates. The basic steps to obtain the dispersion relations closely follow the work by Gandhi et al., which comprehensively addressed Lamb wave acoustoelastic effect [13]. For the bulk waves propagate in hyperelastic material, the stress $\boldsymbol{T}$ and strain relationship can be written as[24]:

$$T_{\alpha\beta} = C_{\alpha\beta\gamma\delta}E_{\gamma\delta} + C_{\alpha\beta\gamma\delta\varepsilon\eta}e^{i}_{\gamma\delta}e_{\varepsilon\eta}, \tag{1}$$

where $\boldsymbol{C}$, $\boldsymbol{E}$, and $\boldsymbol{e}$ represent stiffness tensor, Lagrangian strains, and strain tensor, respectively. $\alpha, \beta, \gamma, \delta, \varepsilon, \eta$ are the indices. For plane stress, $\boldsymbol{T} = \begin{bmatrix} \sigma_{11} & 0 & 0 \\ 0 & \sigma_{22} & 0 \\ 0 & 0 & 0 \end{bmatrix}$ is the corresponding initial stress tensor. The equation of motion of the incremental displacement is given by [24]

$$\frac{\partial}{\partial \xi_\beta}\left[T_{\alpha\beta} + T^{i}_{\beta\gamma}\frac{\partial u_\alpha}{\partial \xi_\gamma} + T_{\beta\gamma}\frac{\partial u^{i}_\alpha}{\partial \xi_\gamma}\right] = \rho^0\frac{\partial^2 u_\alpha}{\partial t^2}, \tag{2}$$

where $\boldsymbol{\xi}$ refers to a natural or unstressed state coordinates, $\boldsymbol{u}^i$ and $\boldsymbol{u}$ represent deformations between the

natural to the initial or static deformation state, and the initial to the final state, respectively. t denotes time. ρ^0 gives the mass density in the natural state.

Providing both material and static pre-deformation are homogeneous, the resulting equation of motion for incremental displacement can be obtained by substituting Eq. (1) to Eq. (2) as follows [24]:

$$A_{\alpha\beta\gamma\delta}\frac{\partial^2 u_\gamma}{\partial\xi_\beta\partial\xi_\delta}=\rho^0\frac{\partial^2 u_\alpha}{\partial t^2}, \tag{3}$$

where

$$\begin{aligned}A_{\alpha\beta\gamma\delta}=&C_{\alpha\beta\gamma\delta}+C_{\beta\delta\varepsilon\eta}e^i_{\varepsilon\eta}\delta_{\alpha\gamma}\\&+C_{\alpha\beta\gamma\delta}\frac{\partial u^i_\gamma}{\partial\xi_\lambda}+C_{\lambda\beta\gamma\delta}\frac{\partial u^i_\alpha}{\partial\xi_\lambda}+C_{\alpha\beta\gamma\delta\varepsilon\eta}e^i_{\varepsilon\eta}\end{aligned} \tag{4}$$

where $\boldsymbol{\zeta}$ is the Kronecker symbol. For the Lamb wave, Eq. (1) can be simplified as [13]:

$$\begin{cases}T_{ij}=B_{ijkl}\frac{\partial u_k}{\partial x_l},\\B_{ijkl}=C_{ijkl}+C_{ijml}e^i_{km}+C_{ijklmh}e^i_{mn},\end{cases} \tag{5}$$

$\boldsymbol{x}$ refers to final state coordinates. Eq. (3) can be simplified as [13]:

$$\begin{aligned}A_{ijkl}=&C_{ijkl}+C_{jlmn}e^i_{mn}\delta_{ik}+C_{ijml}e^i_{km}\\&+C_{mjkl}e^i_{im}+C_{ijklmn}e^i_{mn}.\end{aligned} \tag{6}$$

Therefore, the dispersion relations of symmetric and anti-symmetric modes of Lamb wave can be obtained. For symmetric modes [13]:

$$\begin{aligned}f_s(\omega,c)=&D_{11}G_1\cot(\gamma\alpha_1)+D_{13}G_3\cot(\gamma\alpha_3)\\&+D_{15}G_5\cot(\gamma\alpha_5)=0.\end{aligned} \tag{7}$$

And for anti-symmetric modes:

$$\begin{aligned}f_a(\omega,c)=&D_{11}G_1\tan(\gamma\alpha_1)+D_{13}G_3\tan(\gamma\alpha_3)\\&+D_{15}G_5\tan(\gamma\alpha_5)=0,\end{aligned} \tag{8}$$

where D and G are parameters related to tensor B; $\gamma=\omega d/(2c)$; ω is the angular frequency; d is the thickness of the plate; c is the phase velocity; α is the ratio of the wavenumbers. More detailed discussions and parameters defined in these two equations can be found in Ref. [13]. By solving Eqs. (7) and (8) numerically, the dispersion curves of different Lamb wave modes in the pre-stressed plates can be obtained. However, solving these nonlinear equations is difficult, and complicated iterative numerical methods are needed to search all the roots of these two equations. In addition, such an analytical method can only consider the influence of uniform stress, while varying stress is no longer applicable.

An alternative approach for dispersion analysis is known as the wave finite element (WFE) method to simulate a small segment of the waveguide with periodic boundary conditions based on commercial finite element (FE) codes, as shown in Figure 1. One of the periodic boundaries is based on the Floquet-Bloch (F-B) theory defined by periodic coefficients. The F-B theory provides a strategy to obtain a set of solutions of a linear ordinary equations system with a periodic condition for a certain period. The mathematic relation for the boundary is expressed as [25]:

$$u_{dst}=u_{src}e^{-ik_i\bullet(r_{dst}-r_{src})}, \tag{9}$$

where $\boldsymbol{u}$ is the displacement and $\boldsymbol{r}$ is the distance; *dst* and *src* refer to destination and source plane; k_i refers to incident wavenumber. Therefore, the displacement field on the left side of the unit cell is related to the displacement on the right side. F-B boundary conditions affect only the propagative part of the solution along the direction of wave propagation. Then the dispersion relation can be obtained by tracing the eigenfrequencies for each incident wavenumber k with a fixed length of a small segment. The complicated part of wave propagation is solved by finite element software. The F-B theory has been applied for dispersion analysis of different periodic mechanical systems, especially for the photonic crystal structures [25, 26]. The advantages of this approach over commonly applied analytical methods are obvious. Firstly, the full power of existing commercial FE packages can be well utilized, and existing linear and nonlinear material libraries can be used. Thus, there is no need for extra coding for the different hyperelastic material models. Moreover, various kinds of initial stress states can be introduced conveniently in the FE package with a preload step to simulate the realistic stress field.

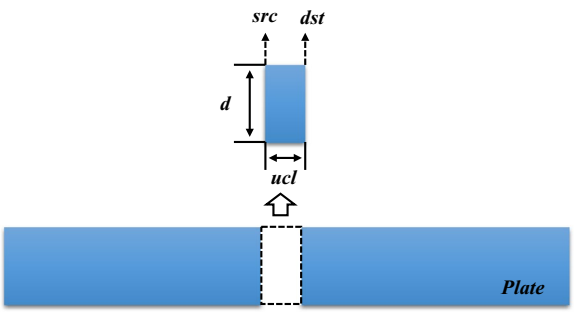

Figure 1 A unit cell in WFE based on F-B theory

3 Dispersion Curves of Lamb Wave Under Uniform Initial Stress

3.1 Calculation of Dispersion Curves Based on F-B Theory

In this study, F-B theory was implemented in a commercial finite element software Comsol Multiphysics. What should be noted is that there is a maximum wavenumber k, corresponding to a minimum wavelength $\lambda_{min} = 2 \cdot ucl$. Therefore, dispersion curves in the high-frequency range should be calculated with a very small unit cell. To ensure sufficient accuracy and convergence, the mesh size and the time step should be strictly chosen [2]. The maximum mesh size was set to 0.02 mm ($N_{min} = \lambda_{min}/0.02 = 10$ for upper-frequency limit 15 MHz). F-B periodic boundary conditions were applied to boundary pairs along the wave propagation. Then, the eigenfrequency f can be calculated for the unit cell for a given incident wavenumber k. Consequently, after sweeping the wavenumber to trace the corresponding eigenfrequencies, full wavenumber-frequency (k-f) pairs are obtained, which can be converted to dispersion curves for phase velocity (c_p-f) and group velocity (c_g-f).

The material is Al6061-T6 same as Ref. [13] for comparison, and the material property is shown in Table 1. The phase velocity and group velocity dispersion curves were obtained for a range of $fd = 0 \sim 15\,\text{MHz} \cdot \text{mm}$ and compared to the Rayleigh-Lamb (R-L) equation, as shown in Figure 2. And in Figure 2, × represents symmetric modes of R-L equation; o represents antisymmetric modes from R-L equation; dash line denotes symmetric modes from F-B theory; line denotes antisymmetric modes from F-B theory. Both phase velocity and group velocity dispersion curves show that F-B theory results match the analytical results by solving the R-L equation; thus, WFE based on F-B theory is validated for dispersion analysis for Lamb wave and will be used for further analysis.

3.2 Acoustoelastic Effect of Uniform Stress on Lamb Wave

The following will investigate the acoustoelastic effect of uniform stress on Lamb waves based on the F-B theory. In order to take the consideration of the acoustoelastic effect of initial stress, which brings in a nonlinear effect in the governing equation, a hyperelastic material model is required. Various models have been developed to account for the elastic contribution to ultrasonic nonlinearity. The difference is how to express the elastic strain energy potential as a function of the Lagrangian strain, leading to nonlinear hyperelastic deformation. The best-known hyperelastic constitutive models include the Neo-Hookean, Mooney–Rivlin, Saint Venant-Kirchhoff, Yeoh, Fung, Ogden, Arruda-Boyce, and Murnaghan models, which can describe the behaviors of hyperelastic materials. Murnaghan's nonlinear model is a popular and classical model to study wave propagation in a quadratic

Table 1 Material properties of Al6061-T6 aluminum plate [13]

Elastic property	Value
Lame's constant $\boldsymbol{\lambda}$ (GPa)	54.308
Lame's constant $\boldsymbol{\mu}$ (GPa)	27.174
Murnaghan constant *l* (GPa)	− 281.5
Murnaghan constant $\boldsymbol{m}$ (GPa)	− 339
Murnaghan constant $\boldsymbol{n}$ (GPa)	− 416
Mass density $\boldsymbol{\rho}$ (kg/m^3)	2704

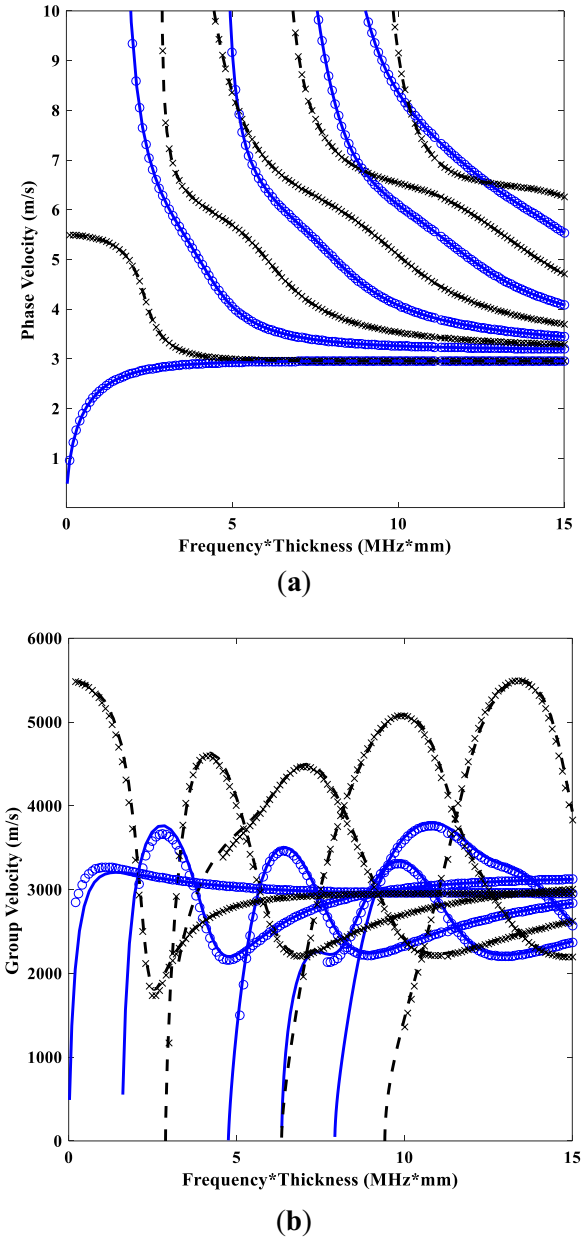

Figure 2 Dispersion curves for Lamb wave in an Al6061-T6 thin plate: (**a**) phase velocity and (**b**) group velocity

nonlinear material. Therefore, the Murnaghan model will be applied in this study. The strain energy density $\boldsymbol{W_s}$ for Murnaghan hyperelastic material is expressed as [27]

$$\begin{aligned} \boldsymbol{W_s} = & \frac{1}{2}(\lambda + 2\mu)\boldsymbol{I}_1(\varepsilon)^2 - 2\mu I_2(\varepsilon) \\ & + \frac{1}{3}(l + 2m)\boldsymbol{I}_1(\varepsilon)^3 \\ & - 2m\boldsymbol{I}_1(\varepsilon)\boldsymbol{I}_2(\varepsilon) + n\boldsymbol{I}_3(\varepsilon)\text{ï¼Œ} \end{aligned} \tag{10}$$

where $\boldsymbol{I}_1$, $\boldsymbol{I}_2$, and $\boldsymbol{I}_3$ are the invariants of the elastic Green-Lagrange strain tensor; λ and μ are the second-order Lame's elastic constants; l, m, and n are the Murnaghan third-order elastic constants.

A stationary preload step introduced a uniform tensile and compressive stress field into this model. Also, hyperelasticity was applied for the pre-deformation because there is a nonlinear relationship between stress and strain in materials, even at tiny deformation. Since higher-order constants affect the strain to a lesser degree, when a tested structure is subjected to substantial deformation, this can lead to significant errors. The application of the Murnaghan hyperplastic material model excludes such simplifying assumptions as the smallness of strain. Moreover, the direction of propagation of the elastic waves was chosen to be parallel to the applied load because it has been proven to exhibit the highest sensitivity of the phase velocity to the applied stress in the case of longitudinal waves.

Therefore, the dispersion curves for phase velocity and group velocity under compressive 100 MPa and tensile 100 MPa were calculated and shown in Figure 3. From the absolute results, the variation in the dispersion curves is not obvious, which is predictable because the previously reported acoustoelastic coefficient is at 10^{-6} MPa. However, somehow it can be seen that the phase velocity of the compressive stress is generally higher than that of the tensile stress, which is consistent with the results of bulk wave and Rayleigh wave acoustoelastic effect [4].

In order to check the influence of different stress levels to compare with previously reported results [13], different uniform stresses with 20, 40, 60, 80, and 100 MPa were studied. Here, the relative variation of phase velocity of A1 and S1 are shown as an example in Figure 4. For each value of the product of frequency and thickness, the velocity variation shows linear change with the stress magnitude. In addition, there is a sharp variation in the

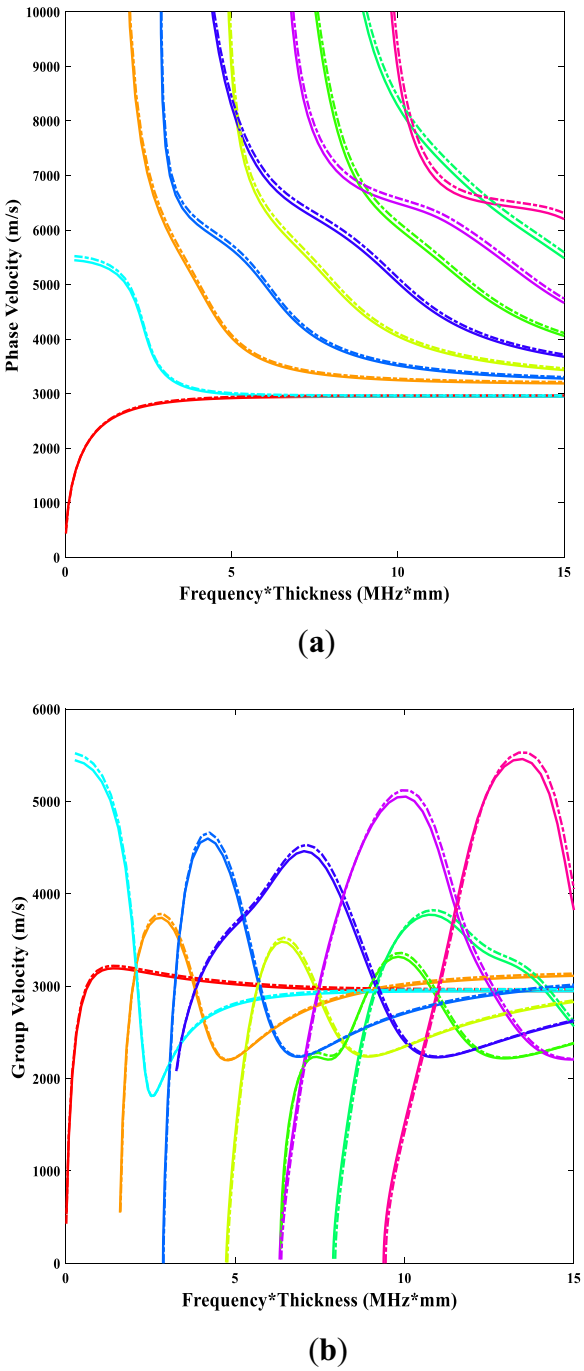

Figure 3 Dispersion curves for Lamb wave propagating along uniform initial stress: (**a**) phase velocity and (**b**) group velocity (solid line: tensile 100 MPa; dash line: compressive 100 MPa)

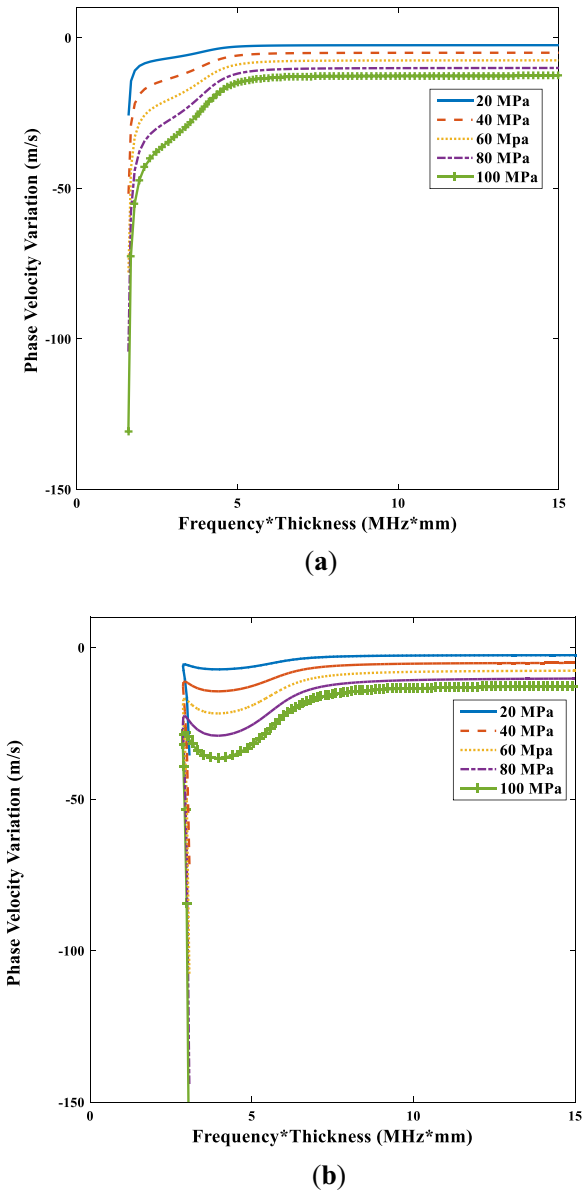

Figure 4 Dispersion curves variation for Lamb wave propagating along different uniform tensile stress of 20 MPa, 40 MPa, 60 MPa, 80 MPa, and 100 MPa: (**a**) for A1 mode and (**b**) for S1 mode

phase velocity of the A1 and S1 modes near their cut-off frequency. In other words, A1 and S1 mode near cut-off frequency is very sensitive to stress. In particular, from the dispersion curves, the frequency-thickness product of S1-ZGV Lamb mode is 2.877 MHz·mm, and it is very close to the S1 cut-off frequency at 3.168 MHz·mm. The closeness between S1-ZGV and cut-off frequency makes S1-ZGV Lamb mode has a high-stress sensitivity. What should be mentioned is that the existence and occurrence of ZGV mode are highly related to the material property. When the material shows a certain degree of inhomogeneity or anisotropy, the occurrence of ZGV mode might change. In this case, the acoustoelastic effect will change accordingly. Since the most widely used ZGV Lamb mode is S1-ZGV mode, which also shows higher excitability than other ZGV Lamb modes [28], this paper only discusses the S1-ZGV mode.

3.3 Effect of Uniform Stress on ZGV Mode

Therefore, the effect of uniform stress on S1-ZGV was studied quantitatively. Here, different uniform stresses ranging from −500 to 500 MPa were considered. The dispersion curves of S1 under compressive 500 MPa and tensile 500 MPa and stress-free are shown in Figure 5. In particular, to study the influence of S1-ZGV, a zoomed view around the frequency of S1-ZGV is shown as well. The results clearly show that the S1-ZGV frequency decreases with tensile stress and increases with compressive stress. This observation indicates that S1-ZGV is sensitive to initial stress, and the shift in frequency is highly possible for stress evaluation.

Further, the frequency shift of S1-ZGV is investigated as a function of stress level. Figure 6 shows the

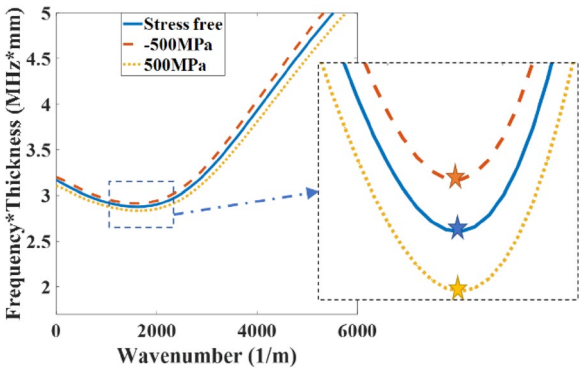

Figure 5 Dispersion curves of S1 mode under different uniform stresses (The stars denote the S1-ZGV mode at stress-free, compressive 500 MPa, and tensile 500 MPa, respectively)

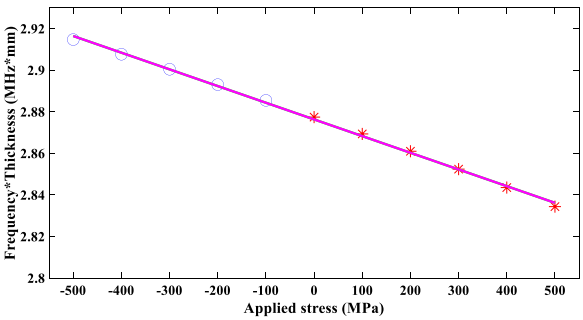

Figure 6 Frequency shift of S1-ZGV Lamb mode under uniform stress (Black circles and red stars denote compressive stress and tensile stress. Red line refers to the fitted curve)

frequency-thickness product of the S1-ZGV mode decrease with different applied stresses. A closely linear relation exists between the stress and the S1-ZGV mode frequency, which is as same as the velocity change in the general acoustoelastic effect. The reason behind it is that the S1-ZGV frequency reflects the phase velocity at a certain wavenumber, and also, there is an empirical formula to derive S1-ZGV from longitudinal wave velocity [29]. Therefore, S1-ZGV is highly potential for stress measurement in plates. The main advantages lie in the two aspects. First, the S1-ZGV frequency is very close to the cut-off frequency, which means that the S1-ZGV mode also possesses high sensitivity to stress measurement compared to other modes. Second, the nature of local characterization based on ZGV mode makes S1-ZGV stress measurement capable of evaluating local stress and reconstructing complex stress fields.

4 Local Stress Measurement in Thin Aluminum Plates

4.1 Numerical Experiments

To demonstrate the feasibility of local stress measurement based on S1-ZGV, numerical studies based on the FE method were carried out. Firstly, a two-dimension FE model was established, as shown in Figure 7. A 3 mm-thick aluminum plate was set to be a hyperelastic material, and the properties are the same as in Table 1. To efficiently generate the S1-ZGV mode in the aluminum plate, which occurs at $fd = 2.877\text{MHz} \cdot \text{mm}$, the center frequency of the excitation signal was chosen as 900 kHz to provide a frequency-thickness product of $2.7\text{MHz} \cdot \text{mm}$ for the 3 mm-thick aluminum plate. Moreover, a relatively wide bandwidth is required to cover the S1-ZGV mode. Therefore, a 3-cycle Hanning windowed sinusoid signal was applied to the plate's upper surface, resulting in a relative bandwidth of 133.33%. The waveform and its spectrum are shown in Figure 8, and the expression is given by:

$$F(t) = (1 - \cos(2\pi ft/3)) \cdot \sin(2\pi ft) \cdot (t < 3f). \quad (11)$$

To ensure stability and convergence, the whole domain was discretized with a maximum mesh of 0.3 mm to cover the frequency of interest. The maximum time increment was set as 8 ns. Furthermore, to reduce the wave reflected from the boundary and avoid building a large model with a large amount of computation, a 15 mm absorbing layer with exponentially increased mass damping parameters was set on both ends of the plate.

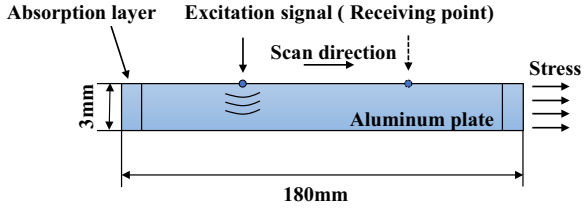

Figure 7 Schematic of the FE model

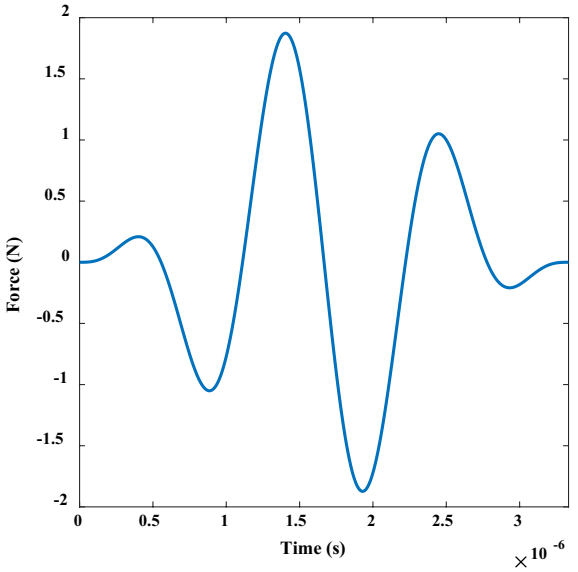

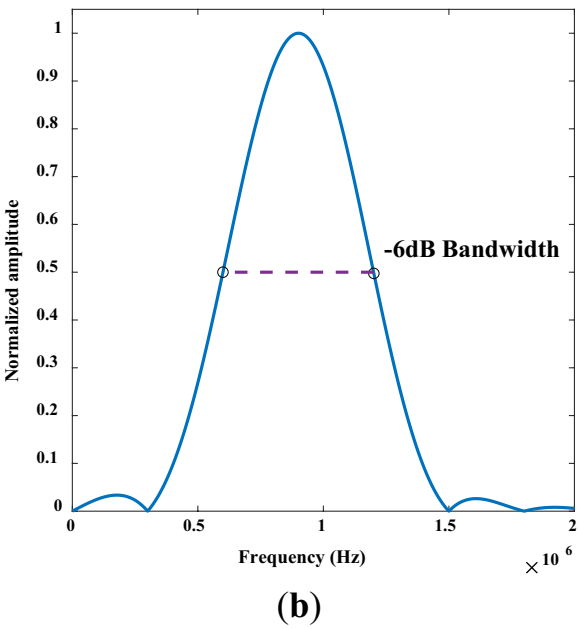

Figure 8 **(a)** Excitation signal of the windowed sinusoid of three cycles, **(b)** frequency spectrum of the excitation signal

A stationary preload step introduced an initial stress field into the plate. At this step, the left side of the plate was set with fixed constraints to ensure convergence. Then, the excitation signal is incident on the upper

surface of the prestressed plate. As the S1-ZGV mode is a local resonance and will not propagate far away from the excitation position, most of the energy is confined within the area of two times the plate thickness [17]. Therefore, a receiver was set near the excitation point to receive the Lamb wave to measure the local stress. The total time of study time was set as 30 μs. Finally, a series of numerical experiments to simulate the scanning measurement will be conducted to reconstruct the complex stress field.

The typical received A-scan signal is shown in Figure 9(a). It consists of a strong direct wave followed by a resonance wave with much lower amplitudes. The direct wave is A0 mode based on single-side excitation, and the resonance wave corresponds to ZGV mode [19]. In order to obtain the accurate frequency of the resonance waves, the direct wave should be removed, similar to the impact-echo method [29]. Figure 9(b) shows the frequency spectrum of the received signals, excluding the direct wave. There is a remarkable peak in the spectrum, and the frequency is 0.959 MHz, corresponding to the product of frequency and thickness $fd = 2.877\text{MHz} \cdot \text{mm}$. It means that the peak corresponds to S1-ZGV mode. Although thickness resonance might exist in this setup, the spectrum shows limited energy at 1.056 MHz, corresponding to the lowest-order longitudinal wave resonance. Hence, the S1-ZGV mode was effectively captured, and its frequency will be applied to stress measurement.

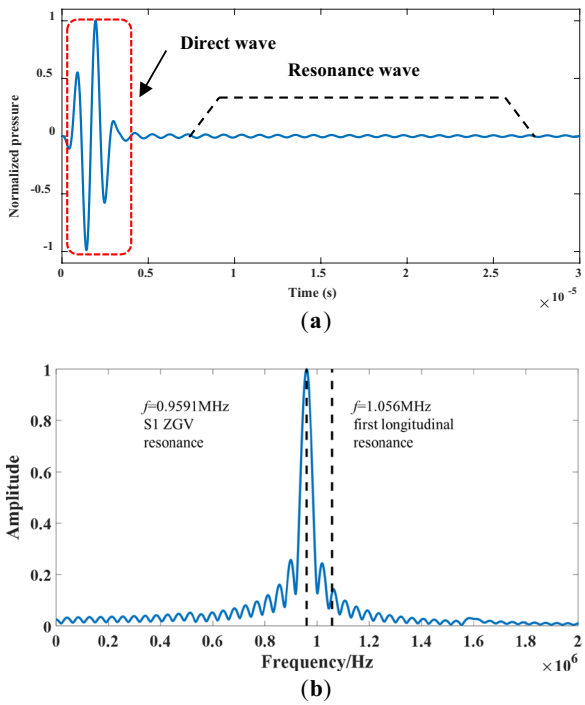

Figure 9 Typical received results: (**a**) A-scan waveforms and (**b**) frequency spectrum of resonance wave

4.2 Relationship Between ZGV Mode Frequency and Applied Stress

To quantitatively measure stress based on S1-ZGV, the relationship between S1-ZGV frequency and stress should be calibrated first. Therefore, a series of uniform tensile stresses ranging from 0 to 300 MPa with an increment of 20 MPa was applied to the plate. Based on the process described in Section 4.1, the relation between calculated S1-ZGV frequency and applied stress was revealed. The results are shown in Figure 10 as the blue dotted line and the predicted result as the yellow solid line from Figure 6. The Y-axis label $\Delta f * d/(f * d)$ represents the variation ratio of the product of S1-ZGV mode frequency and plate thickness. As predicted from the dispersion analysis, it can be observed that the calculated S1-ZGV frequency decreases with increasing tensile stress. However, the change in calculated S1-ZGV frequency is slightly lower than the theoretically predicted results. The reasons for such differences lie in two aspects. First, in numerical experiments, the applied stress is introduced with a preload step to the larger model compared to a small unit cell in Section 3, which will make the deformation not uniform across the whole domain. In addition, the calculated S1-ZGV frequency from numerical experiments might contain extra energy besides the S1-ZGV mode.

It should be noted that only the effect of stress instead of deformation on S1-ZGV mode frequency is considered in this paper. Both reasons will bring some errors in the calculated results from numerical experiments and future practical measurements. Therefore, a calibration of the relationship between calculated S1-ZGV frequency and stress should be addressed. Here, a thickness compensation was adopted to calibrate the results to improve the accuracy based on the following expression [29].

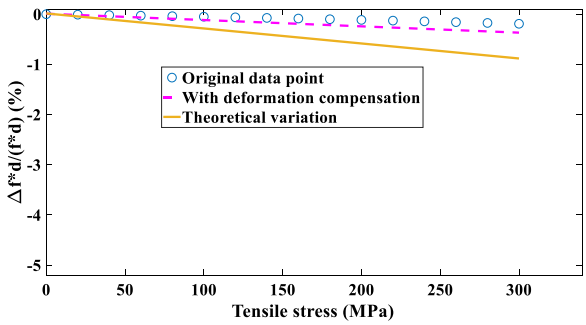

Figure 10 Relative variation of f*d of S1-ZGV with tensile stress. Blue dots refer to original measurement data. Yellow solid line is the theoretical result from dispersion analysis. Pink dash line is the calibrated result with deformation compensation

$$f = \frac{\beta c_L}{2d}, \tag{12}$$

where β is a correction factor defined by ASTM standards, c_L is the longitudinal wave velocity, and d is the thickness of the plate. Providing the correction factor and longitudinal wave velocity are constants, Eq. (12) shows the S1-ZGV frequency shift caused by the thickness deformation during the prestress. Therefore, compensation for the frequency shift will be applied to the original ZGV frequency. The calibrated result after deformation compensation is shown as a pink dashed line. The difference compared to the original result has been reduced. The analytical expression between the tensile stress and S1-ZGV mode frequency is preferable to measure stress quantitatively. Considering a linear regression, the expression of predicted stress σ_p can be established by linear fitting as follows:

$$\sigma_p = s_1 f + s_0, \tag{13}$$

where $\boldsymbol{f}$ is the S1-ZGV mode frequency; the constants $\boldsymbol{s}_1$ and $\boldsymbol{s}_0$ are -0.08383, 8.041×10^4, respectively. Moreover, the correlation coefficient is $\boldsymbol{R}^2 = 0.998$. Therefore, an arbitrary stress field can be measured quantitatively based on this analytical expression.

4.3 Results of Stress Field Measurement

Complex stress fields along the plate were applied to demonstrate the capability of local stress measurement based on the S1-ZGV method. First, concentration stress fields with a Gaussian distribution were introduced in the preload step. A series of numerical experiments ranged from 60 to 120 mm with a step of 2 mm to cover the concentrated stress field. Both tensile and compressive stress were considered with a single localized stress field. Further, more complex stress fields with different peak values and stress gradients were also investigated to discuss the influence of multiple localized stress. Other parameters and data processes were the same as described in Sections 4.1 and 4.2.

4.3.1 Single Localized Stress

Figure 11(a) shows the stress profile along the prestressed plate and the total stress contour. It is a tensile stress field concentrated at the center of the plate, and the peak stress is 200 MPa. With the scanning process, the stress along the plate was measured based on the S1-ZGV method as Eq. (13). Then, the stress distribution was reconstructed and compared to applied stress from 60 to 120 mm. The results show a good agreement, as shown in Figure 11(a).

Similarly, a compressive stress field was introduced and investigated. Figure 11 shows the stress field and its reconstructed stress profile. Also, a good agreement is achieved for this compressive stress field. There is a slight difference around the stress peak compared to the actual stress fields, probably because of the small nonuniformity of deformation and stress distribution through thickness after the preload step. Overall, the good agreement between the reconstructed stress profiles and the actual profiles proves that the proposed S1-ZGV method can accurately reconstruct the stress profile for compressive and tensile stress fields.

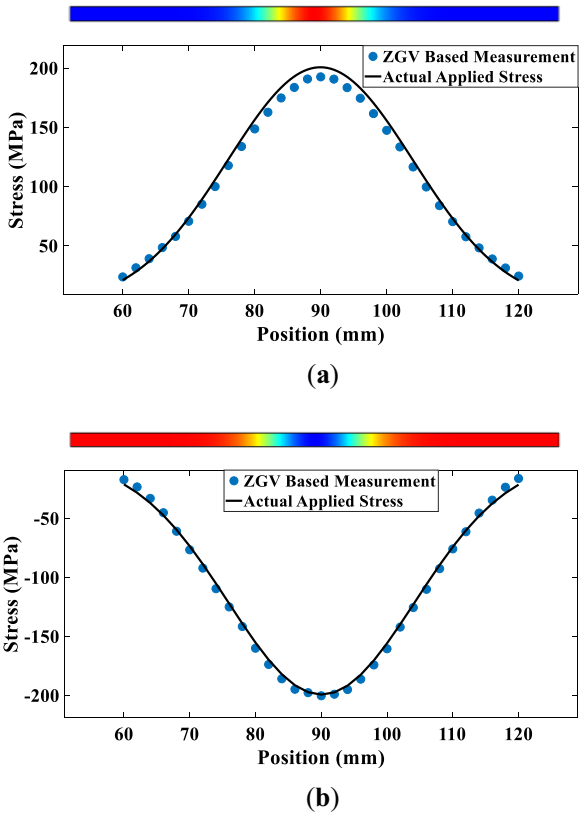

Figure 11 Measurement for localized stress field: (**a**) S1-ZGV based results for tensile stress field, and (**b**) S1-ZGV based results for compressive stress field

4.3.2 Multiple Localized Stresses

Considering the fact that there are much more complex stress fields than the above-discussed cases, multiple localized stresses should be investigated as well. Around the welded zone, the residual stress can be generally regarded as a combination of multiple localized stresses with different peaks and gradients. Therefore, further study was conducted to investigate the feasibility and accuracy of complex stress measurement based on S1-ZGV. In this study, three complex stress fields were introduced in the plate, and the reconstructed stress profiles are shown in Figure 12.

Figure 12(a) shows a stress field combined with two localized stresses with identical stress peaks and gradients. The good agreement indicates that S1-ZGV can identify and localize multiple stresses. To investigate the influence of different peak stresses, two localized stresses with peak stress of 150 MPa and 250 MPa were introduced, and the reconstructed results are shown in Figure 12(b). The results show that the stress peak has little influence on the results. Further, two localized stresses with different ranges were introduced to simulate two stress fields with different stress gradients, and the results are shown in Figure 12(c). The width of the right localized stress is only half of the left. The reconstructed results show a small but non-negligible difference for the right stress, corresponding to the localized stress with a relatively large stress gradient. The reason is that nonuniform stress across the plate increases when the stress gradient increases. Therefore, scanning measurement with small step size and further deformation compensation is required to improve the accuracy of stress measurement for large-gradient stress. Nevertheless, good agreement is achieved for all three stress fields, proving that ultrasonic S1-ZGV stress measurement can identify complex stress fields even with multiple localized stresses.

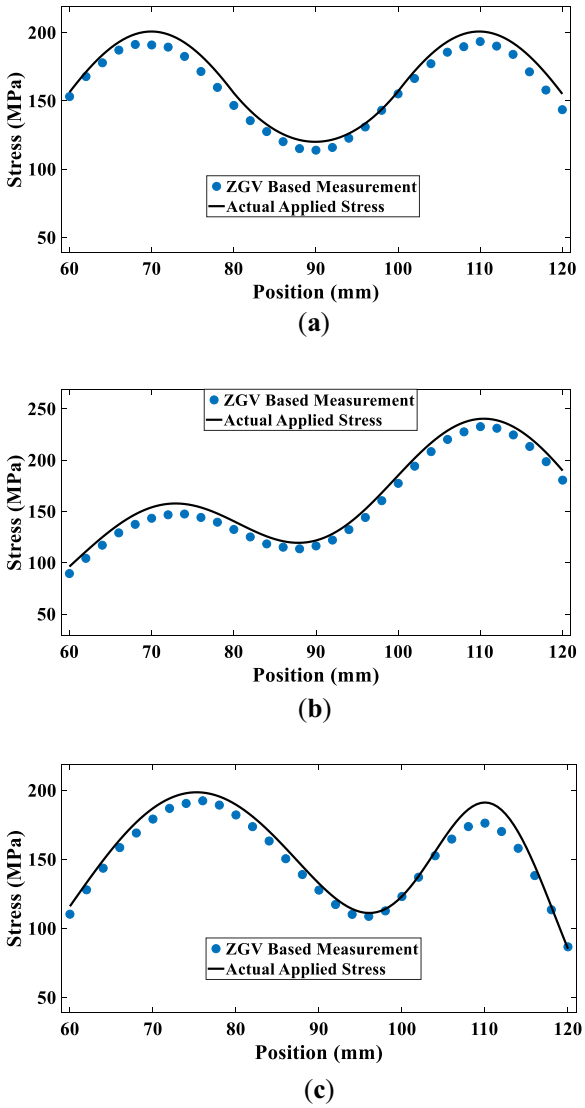

Figure 12 Measurement results for multiple localized stress fields: (**a**) Two localized stresses with identical feature, (**b**) Two localized stress with different stress peak, (**c**) Two localized stress with different stress gradients

5 Conclusions

In this paper, ZGV Lamb wave technology was proposed to measure the local stress field in thin aluminum plates. The main conclusions are summarized as follows.

A) The Acoustoelastic Lamb wave was investigated based on the Floquet-Bloch theory. Dispersion curves obtained for uniform stress show that higher-order Lamb waves near the cut-off frequencies $fd = 3.168\text{MHz} \cdot \text{mm}$ are sensitive to applied stress, indicating that S1-ZGV mode at $fd = 2.877\text{MHz} \cdot \text{mm}$ possesses a rather high sensitivity to stress.

B) Numerical experiments were conducted to simulate the process of stress field measurement. Based on the frequency analysis of the resonance wave, a linear expression between S1-ZGV frequency shift and stress is obtained, along with thickness compensation and linear fitting.

C) A series of numerical experiments were carried out to measure the stress field applied on the plate. Different stress peaks and stress gradients were also considered. The reconstructed results based on the S1-ZGV method agree well with the applied stress profile, proving that the S1-ZGV method is a precise method to measure the complex stress field of the in-service structures.

Further research will be carried out on the experiment validation to prompt practical engineering applications. Also, the influence of anisotropy on the acoustoelastic effect and ZGV mode should be studied for potential application on anisotropic materials such as the composite.

Author contributions

MY and XJ were in charge of the whole project; WX and WX assisted with investigation and data analyses; YC and LZ edited the manuscript. All authors read and approved the final manuscript.

Authors' information

Weiming Xuan, born in 1995, is currently a master candidate at *Guangdong University of Technology, China*. He received his bachelor degree from

Guangdong Polytechnic Normal University, China, in 2018. His research interests include Lamb wave and stress measurement.
Maodan Yuan, born in1988, is currently an assistant professor at *Guangdong University of Technology, China*. He received his PhD degree from *Sungkyunkwan University, Korea.* His research interests include nonlinear ultrasonic technology, guided wave and residual stress measurement.
Xuanrong Ji, is currently a Professor at *Guangdong University of Technology, China*. His current research focus is mainly placed on the novel design and fabrication of piezoelectric transducer, high-frequency ultrasonic array microscopy, phased array ultrasonic, guided wave detection, and large-scale ultrasonic wireless monitoring system.
Wenjin Xu, born in 1995, is currently a master candidate at *Guangdong University of Technology, China.* He received his bachelor degree from *Guangdong Polytechnic Normal University, China,* in 2018. His research interests include guided wave and full waveform inversion.
Yan Chen, is currently an associate professor at *Guangdong University of Technology, China*. She received her PhD degree from *Hong Kong Polytechnic University, China.* Her research interests include piezoelectric ultrasonic transducers and new function material.
Lvming Zeng, born in 1981, is currently an associate research fellow at *Guangdong University of Technology, China*. His current research focuses on laser ultrasound in biomedical imaging and industry inspection.

Funding
Supported by Guangdong Provincial Innovative and Entrepreneurial Research Team Program (Grant No. 2016ZT06G375), National Science Foundation Grants (Grant Nos. 51805097, 51975131, 11804059, 11664011), National Key R&D Program of China (Grant Nos. 2018YFF01010500, 2018YFB1107703), Jiangxi Provincial Science and Technology Program (Grant No. 20171ACB20027).

Availability of data and materials
The datasets supporting the conclusions of this article are included within the article.

Competing interests
The authors declare no conflict of interest.

Received: 19 November 2020 Revised: 21 November 2022 Accepted: 3 February 2023
Published online: 09 March 2023

References

[1] S Kim, Y H Park, S Park, et al. A sensor-type PC strand with an embedded FBG sensor for monitoring prestress forces. *Sensors,* 2015, 15(1): 1060-1070.
[2] M D Yuan, J H Zhang, S J Song, et al. Numerical simulation of Rayleigh wave interaction with surface closed cracks under external pressure. *Wave Motion,* 2015, 57: 143-153.
[3] D S Hughes, J L Kelly. Second-order elastic deformation of solids. *Physical Review,* 1953, 92(5): 1145.
[4] M D Yuan, T Kang, H J Kim, et al. A numerical model for prediction of residual stress using rayleigh waves. *Journal of the KSNT,* 2011, 31: 656-664.
[5] M D Yuan, T Kang, J H Zhang, et al. Numerical simulation of ultrasonic minimum reflection for residual stress evaluation in 2D case. *Journal of Mechanical Science and Technology,* 2013, 27(11): 3207-3214.
[6] Z H Li, J B He, D K Liu, et al. Influence of uniaxial stress on the shear-wave spectrum propagating in steel members. *Sensors,* 2019, 19(3): 492.
[7] W Wang, C H Xu, Y M Zhang, et al. An improved ultrasonic method for plane stress measurement using critically refracted longitudinal waves. *NDT & E International,* 2018, 99: 117-122.
[8] M Mohammadi, J J Fesharaki. Determination of acoustoelastic /acoustoplastic constants to measure stress in elastic/plastic limits by using LCR wave. *NDT & E International*, 2019, 104: 69-76.
[9] Y Javadi, H S Pirzaman, M H Raeisi, et al. Ultrasonic inspection of a welded stainless steel pipe to evaluate residual stresses through thickness. *Materials & Design,* 2013, 49: 591-601.
[10] Y Javadi, M Akhlaghi, M A Najafabadi. Using finite element and ultrasonic method to evaluate welding longitudinal residual stress through the thickness in austenitic stainless steel plates. *Materials& Design*, 2013, 45: 628-642.
[11] S Sadeghi, M A Najafabadi, Y Javadi, et al. Using ultrasonic waves and finite element method to evaluate through-thickness residual stresses distribution in the friction stir welding of aluminum plates. *Materials & Design,* 2013, 52: 870-880.
[12] M Mohabuth, A Kotousov, C T Ng. Effect of uniaxial stress on the propagation of higher-order Lamb wave modes. *International Journal of Non-linear Mechanics,* 2016, 86: 104-111.
[13] N Gandhi, J E Michaels, S J Lee. Acoustoelastic Lamb wave propagation in biaxially stressed plates. *Journal of the Acoustical of Society of America,* 2012, 132(3): 1284-1293.
[14] F Shi, J E Michaels, S J Lee. In situ estimation of applied biaxial loads with Lamb waves. *Journal of the Acoustical of Society of America,* 2013, 133(2): 677-687.
[15] N Pei, L J Bond. Comparison of acoustoelastic Lamb wave propagation in stressed plates for different measurement orientations. *Journal of the Acoustical of Society of America,* 2017, 142(4): EL327 - EL331.
[16] N Pei, L J Bond. Higher order acoustoelastic Lamb wave propagation in stressed plates. *Journal of the Acoustical of Society of America,* 2016, 140(5): 3834-3843.
[17] C Prada, O Balogun, T W Murray. Laser-based ultrasonic generation and detection of zero-group velocity Lamb waves in thin plates. *Applied Physics Letters,* 2005, 87(19): 1066.
[18] H Bjurström, N Ryden. Detecting the thickness mode frequency in a concrete plate using backward wave propagation. *Journal of the Acoustical of Society of America,* 2016, 139(2): 649-657.
[19] C Grünsteidl, T Berer, M Hettich, et al. Determination of thickness and bulk sound velocities of isotropic plates using zero-group-velocity Lamb waves. *Applied Physics Letters,* 2018, 112(25): 251905.1-251905.5.
[20] D Clorennec, C Prada, D Royer. Local and noncontact measurements of bulk acoustic wave velocities in thin isotropic plates and shells using zero group velocity Lamb modes. *Journal of Applied Physics*, 2007, 101(3): 34908.
[21] M Cès, D Royer, C Prada. Characterization of mechanical properties of a hollow cylinder with zero group velocity Lamb modes. *Journal of the Acoustical of Society of America,* 2012, 132(1): 180-185.
[22] J Spytek, A Ziaja-Sujdak, K Dziedziech, et al. Evaluation of disbonds at various interfaces of adhesively bonded aluminum plates using all-optical excitation and detection of zero-group velocity Lamb waves. *NDT& E International,* 2020, 112: 102249.
[23] R. Hodé, S Raetz, J Blondeau, et al. Nondestructive evaluation of structural adhesive bonding using the attenuation of zero-group-velocity Lamb modes. *Applied Physics Letters,* 2020, 116(10): 104101.
[24] Y H Pao, U Gamer. Acoustoelastic waves in orthotropic media. *Journal of the Acoustical of Society of America, 19*85, 77(3): 806-812.
[25] M Collet, M Ouisse, M Ruzzene, et al. Floquet–Bloch decomposition for the computation of dispersion of two-dimensional periodic, damped mechanical systems. *International Journal of Solids and Structures,* 2011, 48(20): 2837-2848.
[26] P Gómez García, J P Fernández-Álvarez. Floquet-bloch theory and its application to the dispersion curves of nonperiodic layered systems. *Mathematical Problems in Engineering*, 2015, 2015: 1-12.
[27] Murnaghan, D Francis. Finite deformations of an elastic solid. *American Journal of Mathematics*, 1937, 59: 235-260.
[28] C Prada, D Clorennec, D Royer. Local vibration of an elastic plate and zero-group velocity Lamb modes. *Journal of the Acoustical of Society of America*, 2008, 124(1): 203-212.
[29] A Gibson, J S Popovics. Lamb wave basis for impact-echo method analysis. *Journal of Engineering Mechanics*, 2005, 131(4): 438-443